Study of basal <a> and pyramidal <c+a> slips in Mg-Y alloys using micro-pillar compression

Wu, Jing; Si, Shanshan; Takagi, Kosuke; Li, Tian; Mine, Yoji; Takashima, Kazuki; Chiu, Yu-Lung

DOI:
10.1080/14786435.2020.1725250

Study of basal <a> and pyramidal <c+a> slips in Mg-Y alloys using micro-pillar compression

Jing Wu[a,*], Shanshan Si[a], Kosuke Takagi[b], Tian Li[a], Yoji Mine[b], Kazuki Takashima[b], Yu Lung Chiu[a]

[a] *School of Metallurgy and Materials, University of Birmingham, Edgbaston, Birmingham, B15 2TT, UK.*

[b] *Department of Materials Science and Engineering, Kumamoto University, 2-39-1 Kurokami Chuo-ku Kumamoto, 860-8555, JAPAN*

** Corresponding author. Email address: wujinguob@163.com (J. Wu)*

Abstract: The effect of yttrium (Y) on the critical resolved shear stresses (CRSS) of <a> basal slip, $\{10\bar{1}2\}\langle\bar{1}011\rangle$ tension twinning and <c+a> pyramidal slip has been studied using micro-pillar compression tests along selected orientations at room temperature, on two magnesium (Mg) alloys with different Y contents (0.4 wt.% and 4 wt.%). The CRSS of <a> basal slip increased slightly from 30±1 MPa (for Mg-0.4Y) to 37±3 MPa (for Mg-4Y). In Mg-0.4Y, the resolved shear stress to activate the $\{10\bar{1}2\}\langle\bar{1}011\rangle$ tension twin was determined to be 45±12 MPa, while in Mg-4Y it was 113 MPa. The compressed samples were studied using scanning electron microscopy (SEM), transmission Kikuchi diffraction (TKD) and transmission electron microscopy (TEM). It was found that <c+a> dislocations slip mainly on $\{\bar{1}\bar{1}22\}$ (Pyra II) planes with a CRSS of about 119 MPa in Mg-0.4Y and slip mainly on $\{0\bar{1}11\}$ (Pyra I) planes in Mg-4Y with a CRSS of 106 MPa. There is a significantly lowered CRSS ratio between <c+a> slip and <a> basal slip in both alloys (2.8 and 4.8) compared with that reported in bulk pure Mg (~100). The easy activation of <c+a> on Pyramidal I slip is expected to promote the frequent cross-slip in Mg-4Y alloy.

Keywords: Mg-Y, micro-pillar compression, CRSS, pyramidal slip, twinning

1. Introduction:

Magnesium is the lightest (with density of 1.73 g/cm^3) structural metal and has wide potential applications in the automotive industries. However, the poor ductility at room temperature limits the use of Mg and its alloys. Partly due to its hexagonally close packed (hcp) structure (c/a ratio of about 1.624), Mg has anisotropic plastic deformation behaviour. For example the CRSS of <c+a> pyramidal slip in pure Mg is about 100 times larger than that of <a> basal slip, and hence <a> basal slip is often the dominant deformation mode [1] which is not able to accommodate the strain along the <c> direction, which is a key reason for the limited ductility of pure magnesium at room temperature.

Recently, it was reported that the addition of rare earth (RE) elements such as Y can significantly improve the ductility of Mg alloys (see for example [2] [3] [4]). It has been recognised that the difference between the CRSS of <c+a> pyramidal slip and <a> basal slip is reduced with Y addition [3] [5] [6] [7]. Sandlöbes et al. [3] [5] studied the dislocation structure in deformed Mg-3 wt.% Y alloy and observed enhanced activation of <c+a> dislocations. Kim et al. [6] reported a study using molecular dynamics (MD) modelling that the CRSS of basal slip increased more than that of pyramidal slip in Mg with Y addition. Wang et al. [8] estimated the CRSS value of the non-basal and basal <a> slips in Mg-3Y alloy using far-field high energy X-ray diffraction, but no CRSS value of <c+a> slips were reported. Kula et al. [9] employed a crystal plasticity model to simulate the deformation of textured Mg-Y alloys and estimated the CRSS value of <a> slip and <c+a> slips. These estimations of CRSS values provides valuable insight to the deformation of Mg-Y alloys, direct measurement of quantitative CRSS results is still urgently demanded. In addition, deformation twinning, which is an important alternative deformation mode to pyramidal slip to accommodate the c-axis strain in pure Mg and its

alloys, has not been well documented in Mg-Y alloys. The effect of Y on the deformation twin in Mg needs to be clarified.

With the development of focussed ion beam (FIB) machining and small-scale mechanical testing techniques, it is possible to perform mechanical testing on miniature single crystal samples extracted from individual grains in polycrystalline samples and thus obtain the CRSS values [10] [11]. For example, using micro-pillar compression, Liu et al. [11] successfully quantified the CRSS of basal slip and tension twinning in pure Mg, and Chen et al. [12] characterised the CRSS of different slip systems in Mg-Zn-Y alloys. So the first aim of this paper is to determine the CRSS of basal <a> slip, tension twin and pyramidal <c+a> slip in Mg-Y samples with different Y additions (0.4 wt.% and 4 wt.% Y) by micro-pillar compression.

The second aim is to study the nature of the <c+a> pyramidal slip in Mg-Y alloys. Although the nucleation, dissociation and active slip planes of <c+a> dislocations in Mg have been studied extensively, there are disagreements or even contradictions in the literature on the nature of the <c+a> dislocations. For instance, the experimental work on pure Mg by Obara et al. [1] suggests <c+a> dislocations slip on $\{\bar{1}\bar{1}22\}$ pyramidal II (Pyra II) plane, which is supported by later work [13] [14]. However, $\{0\bar{1}11\}$ pyramidal I (Pyra I) plane has also been reported as the favourable slip plane for <c+a> dislocation in pure Mg during c-axis compression based on TEM analysis [15], SEM slip trace analysis [16] and modelling work [17] [18]. More recently, Wu et al [19] studied, primarily using atomistic simulation, the <c+a> dislocations in Mg. They reported that Y addition contributes to <c+a> dislocation cross slip. The simulation results were supported by TEM observations obtained from polycrystalline textured samples containing 1 wt.% and 3 wt.% Y. To further clarify the nature of <c+a> slip experimentally, detailed dislocation analyses on the <c+a> dislocations have been carried

out in this work together with the quantitative CRSS values measurement from the single crystal micro-pillar samples.

2. Experimental:

Mg alloys containing 0.4 wt.% and 4 wt.% Y additions were prepared by casting of a mixture of commercial pure Mg and a Mg-30wt.% Y master alloy. The as-cast alloys were sealed in a quartz tube under argon atmosphere and solution treated at 520^{o}C for 96 h, followed by water quenching. The samples were then mechanically polished using 1 µm diamond paste and then electro-polished in the solution containing 10% perchloric acid and 90% ethanol. Electron back-scattered diffraction (EBSD) was carried out using an Oxford Instruments Nordlys EBSD detector attached to a TESCAN MIRA-3 SEM to determine the crystallographic orientation of these samples. Square micro-pillars with typical dimensions of 4.5 µm (length) × 4.5 µm (width) × 9 µm (height) were prepared from selected orientations using an FEI Quanta 3D Focussed Ion Beam (FIB) FEG/SEM system. Micro-pillars were prepared from selected grains with suitable orientations to activate single <a> basal slip, <c+a> slip or $\{10\bar{1}2\}\langle\bar{1}011\rangle$ tension twinning. The loading directions of the prepared pillars and the slip systems expected and their corresponding Schmid factors are shown in *Table 1*. At least three micro-pillars for each condition were compressed using a Hysitron Picoindenter PI85 system (Bruker Corporation) under a nominal strain rate of 2×10^{-3} s^{-1}. The elastic strain accommodated by the diamond indenter and the bulk materials below the pillar were subtracted using Sneddon's equation by considering the punching effect of a cylindrical punch indenting into an elastic half space [12] [20] [21]. The corrected displacement D is obtained using following equation:

$$D = D_{meas} - \frac{1-v_i^2}{E_i}\left(\frac{F_{meas}}{d^t}\right) - \frac{1-v_b^2}{E_b}\left(\frac{F_{meas}}{d_b}\right)$$

Where D_{meas} and F_{meas} are the measured displacement and force; v_i and v_b are the Poisson's ratio of diamond (0.07) and magnesium (0.35) respectively [22] [23]. E_i and E_b are the elastic modulus of the diamond (1143 GPa) and the magnesium (42.9 GPa for 0.4Y-A and 4Y-A micropillars, 50.3 GPa for 0.4Y-C and 4Y-C micropillars, 45.4 GPa for 0.4Y-B and 4Y-B micropillars) [22] [23]. d^t and d_b are the diameters of the top and bottom micropillars. The 0.2% proof stress is taken as the yield strength of the micropillars. The pure elastic part of the compression stress-strain curve is identified when its first derivative remains constant (practically the scattering is less than 10%). The end point of the elastic part is taken as zero strain.

After the compression test, thin foils were then extracted from the compressed micro-pillars using FIB to study the deformation microstructure on an FEI Talos F200 transmission electron microscope (TEM).

Table 1. insert here

3. Results:

3.1 Compression stress-strain curves of Mg-Y micropillars

The engineering stress-strain curves obtained from the micro-pillars are shown in *Figure 1*. Pillars 0.4Y-A and 4Y-A, both in blue colour, show similar plastic flow behaviours with no significant work hardening. The 0.2% proof stress is 70±3 MPa for 0.4Y-A and 103±6 MPa for 4Y-A. The stress-strain curves (in red colour) obtained from pillars 0.4Y-B and 4Y-B appear very different. The curves obtained from 4Y-B pillars are smooth while that from 0.4Y-B pillars show distinct strain bursts followed by high work hardening regions. The 0.2% proof stress of 0.4Y-B pillars appears scattered (67 MPa, 77 MPa, 115 MPa and 132 MPa) compared with that of 4Y-B pillars of about 246 ±5 MPa. The stress-strain curves obtained from 0.4Y-C and 4Y-C pillars (in black) show some

small serrations (which are larger in 4Y-C) and have high work hardening rates compared with those obtained from other groups of pillars. No large strain bursts have been observed on Mg-4Y alloy pillars regardless of the loading directions.

Figure 1 insert here

3.2 SEM and TEM analysis of pillar 0.4Y-A and 4Y-A

Typical SEM images taken from the as-compressed 0.4Y-A pillar (deformed to 8% strain) and 4Y-A pillar (deformed to 6% strain) are shown in *Figure 2a and 2b*, respectively. Both pillars show distinct slip traces parallel to (0001), suggesting that basal <a> slip has been activated. A thin foil parallel to (0001) was extracted from the compressed 4Y-A pillar. Bright field images in *Figure 2c-2f* show long and curved dislocations in the pillar (indicated by the purple dashed curves) and they are out of contrast when imaged using g = $10\bar{1}0$ (*Figure 2e*), implying the Burgers vector of these are <a> dislocations with Burgers vector of $1/3[1\bar{2}10]$, consistent with the fact that $1/3[1\bar{2}10](0001)$ slip system has the largest Schmid factor of 0.36 (Table 1). Based on the 0.2 % proof stress and the Schmid factor, the CRSS of basal <a> slip for Mg-0.4Y and Mg-4Y alloys can be determined to be 30±1 MPa and 37±3 MPa, respectively.

Figure 2 insert here

3.2 TEM analysis of pillar 0.4Y-B

Figure 3 shows the TEM bright-field images obtained from a 0.4Y-B micro-pillar compressed to about 10% strain. The TKD result in *Figure 3b* indicates that twinning has occurred in almost the whole pillar (in blue) except some areas (in red) at the top and bottom of the pillar. The twin has been identified as $\{10\bar{1}2\}\langle\bar{1}011\rangle$ tension twin. The CRSS value for the tension twin in Mg-0.4Y is thus calculated as 45±12 MPa. Under the diffraction vector g = 0002, dense dislocations were observed in the twinned region

indicating that these are not <a> dislocation and that the Burgers vector of these dislocations has a <c> component (*Figure 3a*). The yellow-boxed area in *Figure 3a* is enlarged and shown in *Figure 3c* which shows that many lines parallel to the basal plane on the left part of the image. When imaged using $10\bar{1}1$, fringes of stacking faults can be seen (as shown in *Figure 3d*). The presence of such stacking faults has been widely reported in Mg alloys [24] [25] [26]. A low angle grain boundary along the loading direction in this pillar with the misorientation angle of about 3° can be seen in *Figure 3b*. Images taken along $[1\bar{2}10]$ zone axis were used to study the dislocations in the boundary. As shown in *Figure 3e*, the boundary consists of two groups of straight, parallel dislocations. The dislocations are out of contrast when imaged using g=0002, suggesting these are <a> type dislocations. This type of low angle grain boundary has been frequently observed in Mg-Zn-Y alloys and is recognised as a kink boundary [27] [28]. TKD results indicate that the rotation axis of the low angle grain boundary is $\langle 1\bar{2}10 \rangle$ type, as shown in *Figure 3b*. Yamasaki et al. [28] suggested this type boundary contains two basal <a> slip systems. It is clear lots of stacking faults ended at the kink boundary, which is similar to the morphology where stacking faults left in the wake of advancing the twin boundary [29]. The origin of the kink boundary maybe due to the meeting of two twin variants which has small misorientation angle. The misorientation has been preserved by forming the kinking boundaries. *Figure 3f* shows that this low angle grain boundary effectively blocks dislocations, as pointed by the red arrow.

Although the current compression experiment was performed under constant strain rate, it is likely that the feedback loop used did not offer sufficiently quick response to the large displacement associated with twinning hence the strain bursts observed. Liu et al. [11] observed that an entire pillar was twinned after 5-6% compressive stain. The tensile strain

caused by $\{10\bar{1}2\}\langle 10\bar{1}\bar{1}\rangle$ twin is about 6.5%~6.7% regardless of the twinning mechanism, i.e. the classical shearing mechanism [30] or the atomistic shuffling [31].

Figure 3 insert here

In order to identify the <c> component dislocations observed in the twin region in a compressed pillar of 0.4Y-B, bright-field images with different beam conditions are shown in Figure 4. Taking the arrowed long dislocation as an example, it is in contrast when $g = 0002$ and $g = 10\bar{1}1$, but it is out of contrast when $g = 10\bar{1}0$ and $g = \bar{2}110$. So the Burgers vector of these dislocations are <c> type dislocations. It is interesting to notice that a high density of <c> dislocations is a very common feature in deformation tension twins (see dark areas in *Figure 3*a) and often associated with basal stacking faults. Wang et al. [29] also observed lots of <c>-containing dislocations in the twin, but it was suggested these defects were not caused by the twin boundary movement. Li et al. [26] reported the observation of the <c> dislocations in the Mg twin, no explanation has been given. Agnew et al. [32] suggested a <c> dislocation may be a result of the dissociation of a <c+a> dislocation in a Mg-Li alloy. However, this doesn't explain the direct link between the <c> dislocations and the twins. It is more likely that the <c> dislocations were a residue defect associate with the stacking faults when the twin boundary advanced. <c> dislocation is non-mobile and can't contribute to further strain accommodation.

Figure 4 insert here

3.3 TEM analysis of pillar 4Y-B

Unlike the 0.4Y-B, the deformed 4Y-B micro-pillar with $[\bar{2}7\bar{5}0]$ loading direction shows less twinning. After straining of 8%, the SEM image obtained from the as-compressed pillar (*Figure 5*a) clearly shows a slip trace corresponding to the $(0\bar{1}1\bar{1})$ plane. The corresponding TKD result (*Figure 5*b) confirms that only a small piece of twin exists at

the edge of the sample. A micro-pillar compressed under the same condition but to a smaller strain of 2% was analysed using TEM and the results are shown in Figure 6. The overview image shows a small piece of twin present and the dislocation lines observed are mainly along one direction. As indicated by the yellow line, most straight dislocations are parallel to the trace of $(0\bar{1}11)$. Images obtained from the dashed blue square with different g vectors are shown in Figure 6b-f. Two groups of dislocation can be observed. Group A dislocations are dominant and they are out of contrast when $g = 0\bar{1}1\bar{1}$ and $g = 10\bar{1}0$, suggesting the Burgers vector of $1/3[1\bar{2}13]$. The CRSS for $1/3[1\bar{2}13](0\bar{1}11)$ slip system in Mg-4Y alloys can thus be determined as 106±2 MPa. A second less dense set of dislocations, Group B labelled in Figure 6b, can be observed. Group B dislocations become out of contrast when g vector is $0\bar{1}1\bar{1}$ and $1\bar{1}00$, suggesting they have Burgers vector of $1/3[\bar{1}\bar{1}23]$.

Figure 5 insert here

Figure 6 insert here

3.4 TEM analysis of pillar 4Y-C

The micro-pillar of 4Y-C shows large work hardening during compression. *Figure 7*a shows an SEM image of an as-compressed pillar and the observable slip traces correspond to (0001) indicating <a> type basal slip occurs. The corresponding TEM image in *Figure 7*b indicates that besides basal slip, many dislocations with <c> component also exist. *Figure 7*c shows a long straight basal <a> type dislocation is out of contrast when g=0002 (*Figure 7*d). *Figure 7e and f* are the magnified images of these <c> component dislocations, and they are in contrast when $\mathrm{g} = \bar{2}110$, which confirms they are <c+a> type. Based on the CRSS values measured earlier, the corresponding yield strength for activating <c+a> slip on first pyramidal plane and basal <a> slip along $[01\bar{1}4]$ zone axis

in Mg-4Y can be estimated, which are 220 MPa and 174 MPa respectively. The measured 0.2% proof strength of about 208 MPa is consistent with the activation of <c+a> dislocations, but a little bit higher than the activation of <a> slip. This can be explained by small strain bursts occurring and why slip traces are not obvious in SEM images.

Figure 7 insert here

In order to understand the morphology of the <c+a> dislocations in the 4Y-C pillar, a tilting series has been carried out from -40° to 60° along basal plane (single tilt holder) and the results are in the supplementary video. *Figure 8*c sketches the relative tilting position to the zone axis. Two images with tilting angles of 10° and -40° are shown in *Figure 8*a and 8b. Lots of zig-zag shape dislocations are indicated by yellow in *Figure 8*a and it is likely double cross-slip occurs. After tilting to -40°, these long dislocations appear much shorter; this is consistent with *Figure 5* and *Figure 6* which show that the dominant slip plane is Pyra I plane. It is known that <c+a> dislocations can glide on two Pyra I slip planes and one Pyra II planes as indicated in *Figure 8*c. So it is possible for <c+a> dislocation in Pyra I $(10\bar{1}1)$ plane to cross-slip to Pyra I $(01\bar{1}1)$ or Pyra II $(11\bar{2}2)$ plane. *Figure 8*d illustrates double cross-slip so the zig-zag shape is easier to understand. For clarification, the dislocation part which appears to lie on the basal plane is actually the straight edge or near edge part in Pyra I or Pyra II slip planes.

Figure 8 insert here

3.5 TEM analysis of pillar 0.4Y-C

Figure 9 shows the <c> component dislocations in 0.4Y-C sample in a $(1\bar{2}10)$ section. The <c> component dislocations show distinct morphology difference from 4Y-C micropillar. Lots of dislocation lines appear straight and lie on the basal plane.

Figure 9 insert here

Higher magnification images in *Figure 10* confirm these straight long dislocations are <c+a> dislocation which show contrast with $g = 2\bar{1}\bar{1}0$. There are lots of elongated dislocation loops in *Figure 10* labelled as a, b, c and d. These dislocation loops show contrast with $g = 0002$ and $g = 2\bar{1}\bar{1}0$ and are thus identified as <c+a> dislocations. Dislocation loops b and d are out of contrast when $g = 10\bar{1}\bar{1}$ which indicates the Burgers vector is $1/3[11\bar{2}3]$. Similarly, dislocation loop c is out of contrast when $g = 10\bar{1}1$ which indicates the Burgers vector is $1/3[11\bar{2}\bar{3}]$. It is clear that many <c+a> slip systems are activated in the pillar due to the similar Schmid factors. To further investigate the possible slip plane, a (0001) section is shown in Figure 11. Figure 11a shows lots of straight dislocations and these dislocations are out of contrast when $g = \bar{1}10\bar{1}$ and $g = 01\bar{1}\bar{1}$, so the Burgers vector is determined as $1/3[\bar{1}2\bar{1}3]$. These dislocations are parallel to the trace of $(\bar{1}2\bar{1}1)$, and according to Figure 9 and Figure 10, straight parts of the <c+a> dislocations are likely to lie on (0001) as well. So the dislocation line directions are $[10\bar{1}0]$. The slip plane contains line directions of $[10\bar{1}0]$ and $[\bar{1}2\bar{1}3]$, which can be identified as $(1\bar{2}12)$ (Pyra II plane). The straight part of the dislocation is an edge section and a schematic drawing of a typical <c+a> dislocation loop in 0.4Y-C pillar is shown on Figure 11d.

Figure 10 insert here

Figure 11 insert here

4. Discussion

4.1 Effect of Y addition on the Twinning

Different deformation modes were observed in 0.4Y-B and 4Y-B pillars when deformed along $[\bar{2}7\bar{5}0]$. With 0.4%Y, the Mg alloy was mainly deformed by $\{10\bar{1}2\}$ tension twinning with a corresponding CRSS of 45±12 MPa. When the Y content was increased to 4%, the twinning tendency reduced and instead <c+a> dislocations became dominant

and only a small piece of twin was observed in the deformation microstructure. Assuming the small piece of twinning was generated when the plastic yielding occurs the CRSS for $\{10\bar{1}2\}$ tension twin of Mg-4Y would be 113 MPa. The increasing CRSS for the tension twin with increasing Y content needs to be understood.

The stress needed for twin nucleation and that for growth (boundary migration) may have different values. For example, B. Liu et al. [33] reported comparable stress values for twin nucleation and for boundary migration while Y. Liu et al. [11] observed a larger stress needed for twin nucleation than that for boundary migration in pure Mg. In the current study, the twinning was associated with the large strain burst in Mg-0.4Y alloy and at the end of the strain burst, the twin boundary migration has already finished. This suggests that the twin boundary migrated at high speed or in other words the stress needed for twin boundary migration should be no larger (likely smaller) than the stress required for twin nucleation. Therefore, the fact that only a small piece of twin was observed in the deformed sample in Mg-4Y (*Figure 5* and *Figure 6*) implies that the twin has not gone through the same rapid growth as that in Mg-0.4Y. In other words, the growth of twin boundary in Mg-4Y would requires higher stress than 113 MPa, which is greater than the CRSS for <c+a> pyramidal slip.

Mendelson [34] suggested that non-planar dislocation dissociations can result in the formation of a twin embryo. The pole mechanism (see for example Hirth and Lothe [35]) also requires the dissociation of <c+a> dislocations into zonal twin dislocations and colinear partials. It is known that the dislocation dissociation can be promoted by reducing SFE. Both TEM analysis and DFT calculation suggests that the SFE can be reduced by Y addition in Mg-Y alloys [5]. This indicates that Y addition is likely to facilitate twin embryo formation. For twin boundary migration, mobile dislocation [36] and atomic shuffling [37] are the main competing mechanisms reported in bulk Mg alloys. Liu et al. [33]

suggested twin boundary migration occurs by basal/prismatic transformation via local rearrangements of atoms in sub-micron Mg samples. Stanford et al. [38] suggested the larger Y atoms inhibit the shuffle process required for twin boundary migration and therefore it is possible that the Y increases the activation stress needed for twin boundary migration. In other words, the twinning deformation in Mg-Y alloys is probably affected by not only the stacking fault energy but also by the concentration of the solute element. Furthermore, Y addition to the system may also alter the relative ease for both <a> basal and <c+a> pyramidal dislocation slip which as competitive deformation mechanisms may also affect the activation and growth of the twinning. Although the fact that the CRSS value of 45 MPa for the tension twinning measured in 0.4Y-B sample being much larger than that of 2 MPa in pure Mg [39] and rarity in 4Y-B sample seems contradicting the expectation on the reduced SFE upon increasing Y content, it is probably a result caused by the overshadowing of the reduced SFE by the inhibited atomic shuffling during the twin, and the change of the relative ease of some dislocation movement, all due to the increased Y content. Future combinatory study on these effects will be useful to understand the twinning deformation in Mg-Y alloys.

The scattering of critical stress measured on tension twinning is 12 MPa (ie. 26%) which is much larger than those measured on pillars which deform by dislocation slip (5%) might be caused by the local stress concentration possibly experienced during the experiment at locations such as between the indenter and the sample surface [11].

4.2 Effect of Y addition on <c+a> dislocations

When compressed along the direction close to the c-axis, <c+a> dislocations were profuse in the deformed alloys. This is in strong contrast to observations in pure magnesium but suggests easy activation of the <c+a> dislocations in the Mg-Y alloys, which agrees with previous reports [5]. Sandlöbes et al. [5] suggested that the formation of non-basal slip was due to the stacking faults in Mg-3% Y alloy. However, uncertainty remains on the

nucleation of non-basal slip in Mg alloys. For instance, Agnew et al [40] postulated that <c+a> dislocations were formed by the dissociation of a $1/6\langle 20\bar{2}3\rangle$ dislocation associated with a pre-existing I1 stacking fault, which also produces another $1/6\langle 20\bar{2}3\rangle$ stair rod dislocation. Recently, the nucleation of <c+a> dislocations was also suggested to be the result of unfaulting of two I1 stacking faults on the basal plane [24], following the reaction $1/6\langle 20\bar{2}3\rangle + 1/6\langle 02\bar{2}3\rangle \rightarrow 1/3\langle 11\bar{2}3\rangle$. However, as shown in Figure 10(a), small <c+a> dislocation loops have been observed in the deformed 0.4Y-C pillar loaded close to [0001]. Hence it is very likely that the <c+a> dislocations are generated directly during the plastic deformation, rather than via the transformation from other defects (dislocation or stacking fault) as mentioned above.

It is of interest to note that the dominant slip plane for <c+a> dislocations changed from Pyra II slip plane in Mg-0.4Y alloy to Pyra I slip plane in Mg-4Y alloy. <c+a> dislocations also show different morphologies. <c+a> dislocations glide in Pyra II slip plane in Mg-0.4Y alloy tend to have long edge segment and short screw segment. This indicates that the mobility of the edge segment is low. On the other hand, double cross-slip between Pyra I and Pyra I or Pyra II plane has been frequently observed in Mg-4Y alloy. The current results agree with Wu et al. [19] that increasing Y content promotes the <c+a> dislocation cross slip and suggested it as an important reason for the Y-induced ductility increase.

4.3 Size effect on the CRSS value

The CRSS values of different slip systems in Mg-0.4Y and Mg-4Y are summarised in Table 2. A strong sample size effect on the strength of Mg has been extensively reported when the sample size was reduced to micron or sub-micron levels [11] [41] . For example,

a significant sample size effect was reported for those samples of 2.5 μm or smaller [41] [42] and also varies with crystallographic orientations [42].

Uchic et al. [43] and Liu et al. [11] reported the strength of a bulk sample can be manifested by micro-pillar when the sample size reach 10 μm. If the fitting coefficient n value of -0.49 is applied to correct the current work, the CRSS value for basal slip is 21 and 26 for Mg-0.4Y and Mg-4Y with size of 10 μm respectively. For pyramidal <c+a> slip, Byer et al. [42] studied the micro-pillars compressed along [0001] zone axis and a reduced size effect with n value of -0.2 is reported. By applying n value of -0.2 for the current study, the CRSS for pyramidal <c+a> slip for Mg-0.4Y and Mg-4Y with size of 10 μm are 101 MPa and 90 MPa respectively.

Prasad et al [44] carried out compression work on Mg orientated for twinning with sample size of 3 μm and 3 mm and observed no significant size dependence on the tension twin CRSS. This is supported by Liu et al [11] where no size effect is observed on twin in the range of 3-10 μm. However, the in-situ TEM compression work carried out by Ye et al. [41] suggested an activating stress of about 1.26 GPa for tension twin and it is significantly larger than the bulk sample which indicates a strong size effect exists. Yu et al. [45] [46] also reported a size effect on twin deformation in both Mg and Ti. Due to the inconsistency of these works, the size effect of the deformation twin is still an open question. So in the current work, the CRSS for the twin will not be modified.

4.4 Effect of Y addition on the CRSS for <a> basal and <c+a> pyramidal slips

Y addition has an obvious strengthening effect as has been reported previously [9], which is probably due to the solution strengthening of Y [47]. The Mg-0.4Y micro-pillar has an CRSS of about 30 MPa (derived from the 0.2% proof stress), in contrast to the resolved

shear stress of 30 MPa (based on the 2% flow stress) in pure Mg of 3 um [44] and of 6 MPa for pillars of 10 um size [11].

More interesting is the effect of Y addition on the ratio between the CRSS of <c+a> pyramidal slip and that of <a> basal slip. The ratio between the CRSS of <c+a> pyramidal slip and that of <a> basal slip for Mg-0.4Y and Mg-4Y is about 4 and 2.83, respectively. This is shown in Figure 12 together with those available in the literature. The currently measured values are much lower than the ratio of 100 for pure Mg, but higher than that computed using molecular dynamics which is less than 2 for the alloy containing 1 at.% Y (i.e. ~3.6 wt.%) [6]. Although the exact reason is unknown, this discrepency is between two at very different strain rates and temperatures. Also it should be noted that the molecular dynamics modelling was based on pure edge disloction only.

Table 2 insert here

Figure 12 insert here

It is worth mentioning that the difference between <c+a> to <a> ratios in Mg-0.4Y and Mg-4Y is quite small. On the contrary, the large difference between CRSS for twin formation in both samples will play an important role on the overall deformation modes for polycrystalline samples. It is expected more deformation twinning exists in alloys with less Y addition.

5. Conclusions

(1) The CRSS of the basal <a> slip increased slightly from 30±1 MPa (Mg-0.4Y) to 37±3 MPa (Mg-4Y), presumably due to solid solution strengthening.

(2) The CRSS for tension twinning (>120 MPa) in Mg-4Y is significantly larger than Mg-0.4Y, which has a CRSS value of 45±12 MPa. It is likely the higher Y content significantly inhibits twin boundary movement thus result in an increasing of CRSS.

(3) The active slip plane for <c+a> dislocations in Mg-0.4Y is Pyra II plane with CRSS value of 119±2 MPa while the active slip plane for <c+a> dislocations in Mg-4Y is Pyra I plane with CRSS value of 106±2 MPa. The CRSS values for both slip systems are similar.

(4) The ratios between CRSS values of non-basal slip to that of basal slip in both alloys (2.8~4.8) are significantly reduced compared to pure Mg (~100). This indicates that non-basal slip systems are more active in Mg-Y alloys, which together with the less active deformation twinning than non-basal slip in Mg-4Y contribute to the improved overall ductility reported in Y-containing Mg alloys.

Acknowledgement

The authors acknowledge the support from the Engineering and Physical Science Research Council for funding (EP/L017725/1) for some facilities used in this work. The authors would like to thank Professors Mike Loretto and Ian Jones for helpful discussions on the paper.

References

[1] T. Obara, H. Yoshinga, S. Morozumi, $\{11\bar{2}2\}\langle\bar{1}\bar{1}23\rangle$ slip system in magnesium, Acta Metall. **21**(7) (1973) 845-853.

[2] T. Al-Samman, X. Li, Sheet texture modification in magnesium-based alloys by selective rare earth alloying, Mater. Sci. Eng. A **528**(10) (2011) 3809-3822.

[3] S. Sandlöbes, S. Zaefferer, I. Schestakow, S. Yi, R. Gonzalez-Martinez, On the role of non-basal deformation mechanisms for the ductility of Mg and Mg–Y alloys, Acta Mater. **59**(2) (2011) 429-439.

[4] N. Stanford, D. Atwell, M.R. Barnett, The effect of Gd on the recrystallisation, texture and deformation behaviour of magnesium-based alloys, Acta Mater. **58**(20) (2010) 6773-6783.

[5] S. Sandlöbes, M. Friák, S. Zaefferer, A. Dick, S. Yi, D. Letzig, Z. Pei, L.F. Zhu, J. Neugebauer, D. Raabe, The relation between ductility and stacking fault energies in Mg and Mg–Y alloys, Acta Mater. **60**(6–7) (2012) 3011-3021.

[6] K.-H. Kim, J.B. Jeon, N.J. Kim, B.-J. Lee, Role of yttrium in activation of <c + a> slip in magnesium: an atomistic approach, Scripta Mater. **108** (2015) 104-108.

[7] Z. Huang, L. Wang, B. Zhou, T. Fischer, S. Yi, X. Zeng, Observation of non-basal slip in Mg-Y by in situ three-dimensional X-ray diffraction, Scripta Mater. **143** (2018) 44-48.

[8] L. Wang, Z. Huang, H. Wang, A. Maldar, S. Yi, J.-S. Park, P. Kenesei, E. Lilleodden, X. Zeng, Study of slip activity in a Mg-Y alloy by in situ high energy X-ray diffraction microscopy and elastic viscoplastic self-consistent modeling, Acta Materialia, **155** (2018) 138-152.

[9] A. Kula, X. Jia, R.K. Mishra, M. Niewczas, Flow stress and work hardening of Mg-Y alloys, Inter. J. Plasticity, **92** (2017) 96-121.

[10] J.R. Greer, J.T.M. De Hosson, Plasticity in small-sized metallic systems: Intrinsic versus extrinsic size effect, Prog. Mater. Sci. **56**(6) (2011) 654-724.

[11] Y. Liu, N. Li, M. Arul Kumar, S. Pathak, J. Wang, R.J. McCabe, N.A. Mara, C.N. Tomé, Experimentally quantifying critical stresses associated with basal slip and twinning in magnesium using micropillars, Acta Mater. **135** (2017) 411-421.

[12] R. Chen, S. Sandlöbes, C. Zehnder, X. Zeng, S. Korte-Kerzel, D. Raabe, Deformation mechanisms, activated slip systems and critical resolved shear stresses in an Mg-LPSO alloy studied by micro-pillar compression, Materials & Design, **154** (2018) 203-216.

[13] B. Syed, J. Geng, R. K. Mishra, K. S. Kumar, [0001] Compression response at room temperature of single-crystal magnesium, Scripta Mater. **67**(7) (2012) 700-703.

[14] E. Lilleodden, Microcompression study of Mg (0001) single crystal, Scripta Mater. **62**(8) (2010) 532-535.

[15] C.M. Byer, B. Li, B. Cao, K.T. Ramesh, Microcompression of single-crystal magnesium, Scripta Mater, **62**(8) (2010) 536-539.

[16] K.Y. Xie, Z. Alam, A. Caffee, K. J. Hemker, Pyramidal I slip in c-axis compressed Mg single crystals, Scripta Mater. **112** (2016) 75-78.

[17] Y. Tang, J.A. El-Awady, Formation and slip of pyramidal dislocations in hexagonal close-packed magnesium single crystals, Acta Mater. **71** (2014) 319-332.

[18] B. Li, E. Ma, Pyramidal slip in magnesium: Dislocations and stacking fault on the $\{10\bar{1}1\}$ plane, Philos. Mag. **89**(14) (2009) 1223-1235.

[19] Z. Wu, R. Ahmad, B. Yin, S. Sandlöbes, W.A. Curtin, Mechanistic origin and prediction of enhanced ductility in magnesium alloys, Science, **359**(6374) (2018) 447-452.

[20] L. Jiang, N. Chawla, Mechanical properties of Cu_6Sn_5 intermetallic by micropillar compression testing, Scripta Materialia, 63 (2010) 480-483.

[21] I.N. Sneddon, The relation between load and penetration in the axisymmetric boussinesq problem for a punch of arbitrary profile, Int. J. Eng. Sci., 3 (1965) 47-57.

[22] G. Simmons, H. Wang, Single crystal elastic constants and calculated aggregate properties: a handbook, MIT Press, Cambridge, MA (1971)

[23] M. Tane, Y. Nagai, H. Kimizuka, K. Hagihara, Y. Kawamura, Elastic properties of an Mg–Zn–Y alloy single crystal with a long-period stacking-ordered structure, Acta Materialia, **61** (2013) 6338-6351.

[24] S.Q. Zhu, S.P. Ringer, On the role of twinning and stacking faults on the crystal plasticity and grain refinement in magnesium alloys, Acta Mater. **144** (2018) 365-375.

[25] X. Wang, L. Jiang, A. Luo, J. Song, Z. Liu, F. Yin, Q. Han, S. Yue and J.J. Jonas, Deformation of twins in a magnesium alloy under tension at room temperature, J. Alloys Compd. **594** (2014) 44-47.

[26] B. Li, P.F. Yan, M.L. Sui, E. Ma, Transmission electron microscopy study of stacking faults and their interaction with pyramidal dislocations in deformed Mg, Acta Mater. **58**(1) (2010) 173-179.

[27] X.H. Shao, Z.Q. Yang, X.L. Ma, Strengthening and toughening mechanisms in Mg-Zn-Y alloy with a long period stacking ordered structure, Acta Mater. **58**(14) (2010) 4760-4771.

[28] M. Yamasaki, K. Hagihara, S.-i. Inoue, J.P. Hadorn, Y. Kawamura, Crystallographic classification of kink bands in an extruded Mg–Zn–Y alloy using intragranular misorientation axis analysis, Acta Mater. **61**(6) (2013) 2065-2076.

[29] F. Wang, C.D. Barrett, R.J. McCabe, H. El Kadiri, L. Capolungo, S.R. Agnew, Dislocation induced twin growth and formation of basal stacking faults in $\{10\bar{1}2\}$ twins in pure Mg, Acta Materialia, 165 (2019) 471-485.

[30] J.W. Christian, S. Mahajan, Deformation twinning, Prog. Mater. Sci. **39**(1) (1995) 1-157.

[31] B. Li, X.Y. Zhang, Global strain generated by shuffling-dominated $\{10\bar{1}2\}\langle 10\bar{1}\bar{1}\rangle$ twinning, Scripta Mater. **71** (2014) 45-48.

[32] S.R. Agnew, J.A. Horton, M.H. Yoo, Transmission electron microscopy investigation of $\langle$c+a$\rangle$ dislocations in Mg and α-solid solution Mg-Li alloys, Metall. Mater. Trans. A, 33 (2002) 851-858.

[33] B.-Y. Liu, J. Wang, B. Li, L. Lu, X.-Y. Zhang, Z.-W. Shan, J. Li, C.-L. Jia, J. Sun, E. Ma, Twinning-like lattice reorientation without a crystallographic twinning plane, Nat. Commun. **5** (2014) 3297.

[34] S. Mendelson, Dislocation dissociations in hcp metals, J Appl. Phys. **41**(5) (1970) 1893-1910.

[35] J.P. Hirth, J. Lothe, Theory of Dislocations, 2nd ed. John Wiley & Sons, New York, 1982.

[36] A. Serra, D.J. Bacon, A new model for $\{10\bar{1}2\}$ twin growth in hcp metals, Philos. Mag. A, **73**(2) (1996) 333-343.

[37] B. Li, E. Ma, Atomic shuffling dominated mechanism for deformation twinning in magnesium, Phys. Rev. Lett. **103**(3) (2009) 035503.

[38] N. Stanford, R.K.W. Marceau, M. R. Barnett, The effect of high yttrium solute concentration on the twinning behaviour of magnesium alloys, Acta Mater. **82** (2015) 447-456.

[39] R.E. Reed-Hill, W.D. Robertson, Additional modes of deformation twinning in magnesium, Acta Metall. **5**(12) (1957) 717-727.

[40] S.R. Agnew, L. Capolungo, C.A. Calhoun, Connections between the basal I1 "growth" fault and ⟨c + a⟩ dislocations. Acta Mater. **82** (2015) 255-265.

[41] J. Ye, R.K. Mishra, A.K. Sachdev, A.M. Minor, In situ TEM compression testing of Mg and Mg–0.2 wt.% Ce single crystals, Scripta Mater. **64**(3) (2011) 292-295.

[42] C. M. Byer, K.T. Ramesh, Effects of the initial dislocation density on size effects in single-crystal magnesium, Acta Mater, **61**(10) (2013) 3808-3818.

[43] M.D. Uchic, D.M. Dimiduk, J.N. Florando, W.D. Nix, Sample dimensions influence strength and crystal plasticity. Science, 2004. **305**(5686) 986-989.

[44] K.E. Prasad, K. Rajesh, U. Ramamurty, Micropillar and macropillar compression responses of magnesium single crystals oriented for single slip or extension twinning, Acta Mater. 65 (2014) 316-325

[45] Q. Yu, L. Qi, K. Chen, R.K. Mishra, J. Li, A.M. Minor, The Nanostructured Origin of Deformation Twinning, Nano Letters, **12**(2) (2012) 887-892.

[46] Q. Yu, Z.W. Shan, J. Li, X. Huang, L. Xiao, J. Sun, E. Ma, Strong crystal size effect on deformation twinning. Nature, 2010. **463**(7279) 335-338.

[47] A. Akhtar, E. Teghtsoonian, Solid solution strengthening of magnesium single crystals—I alloying behaviour in basal slip, Acta Metall. **17**(11) (1969) 1339-1349.

[48] J. Wang, N. Stanford, Investigation of precipitate hardening of slip and twinning in Mg5%Zn by micropillar compression, Acta Mater. **100** (2015) 53-63.

[49] N. Stanford, R. Cottam, B. Davis, J. Robson, Evaluating the effect of yttrium as a solute strengthener in magnesium using in situ neutron diffraction, Acta Mater. **78** (2014) 1-13.

Table captions:

Table 1: Details of the micro-pillars prepared in the current study.

Table 2: CRSS values of different slip systems determined from Mg-0.4Y and Mg-4Y micro-pillars and those from pure Mg in bulk form and micro-sized pillars reported in the literature.

Table 1

Alloys	Pillars	Loading direction	Expected slip/twinning system	Schmid factor
Mg-0.4Y	0.4Y-A	$[47\bar{1}\bar{1}\ \bar{1}8]$	$1/3\langle 1\bar{2}10\rangle(0001)$	0.43
	0.4Y-B	$[\bar{2}7\bar{5}0]$	$\{10\bar{1}2\}\langle\bar{1}011\rangle$	0.46
	0.4Y-C	$[\bar{1}2\bar{1}18]$	$1/3\langle\bar{1}\bar{1}23\rangle\{11\bar{2}2\}$	0.46
Mg-4Y	4Y-A	$[\bar{2}7\bar{5}3]$	$1/3\langle 1\bar{2}10\rangle(0001)$	0.36
	4Y-B	$[\bar{2}7\bar{5}0]$	$\{10\bar{1}2\}\langle\bar{1}011\rangle$	0.46
	4Y-C	$[01\bar{1}4]$	$1/3\langle\bar{1}\bar{1}23\rangle\{01\bar{1}1\}$	0.48

Table 2

	<a> (MPa)	<c+a> (MPa)	$\{10\bar{1}2\}\langle\bar{1}011\rangle$ Twin (MPa)
Mg-0.4Y	30±1	119±2, $\langle\bar{1}\bar{1}23\rangle\{11\bar{2}2\}$	45±12
Mg-4Y	37±3	106±2, $\langle 11\bar{2}3\rangle\{10\bar{1}1\}$	> 113 *
Pure Mg (bulk)	0.52-0.81 [48]	~50 [1], $\langle\bar{1}\bar{1}23\rangle\{11\bar{2}2\}$	2 [39]
Pure Mg (Micro-pillars)	54-68 (1.6 μm) [41] 39-68 (3 μm) [42] 30±5 (3μm) [47] 6 (10 μm) [11]	~135, (2.1 μm) $\langle\bar{1}\bar{1}23\rangle\{11\bar{2}2\}$ [14] ~76, (6.1 μm) $\langle\bar{1}\bar{1}23\rangle\{11\bar{2}2\}$ [14]	~260 (100 nm) [45] 59 (3-10 μm) [11] 55-74 (3 μm, 3 mm) [47]

*Note: Tension twin stops growing at this stress in Mg-4Y alloy.

Figure captions:

Figure 1: compression stress-strain curves obtained from Mg-0.4Y micro-pillars (a) and Mg-4Y micro-pillars (b) along different loading directions shown in Table 1

Figure 2: SEM images obtained from the compressed 0.4Y-A pillar (a) and 4Y-A pillar (b) showing the slip traces parallel to (0001) plane. (c-f) TEM bright field images obtained from 4Y-A pillar under different two-beam conditions. The foil normal is close to [0001]. The purple curves indicate the dislocation lines with Burgers vector $1/3[1\bar{2}10]$.

Figure 3: (a) Overview TEM bight field image of as compressed pillar 0.4Y-B; (b) a TKD image shows the deformed micro-pillar with large volume of twins. Red represents matrix, blue represents twinning and green represents area failed to index which is mainly the surrounding Pt coating; (c) bright field image of the enlarged area in Fig 3a shows the <c> component dislocations. Beam direction (BD) close to $[1\bar{2}10]$; (d) bright field image showing stacking fault; (e) bright field image under multiple-beam condition with BD~$[1\bar{2}10]$ showing geometry necessary dislocations in the low angle boundary. Parallel arrows indicate two dislocation line directions; (f) bright field image showing dislocations (as arrowed) stopped by the low angle boundary.

Figure 4: Bright-field images of an enlarged area in compressed pillar 0.4Y-B with different g vectors showing dislocation with <c> Burgers vector. (a)(b)(d) BD~ $[1\bar{2}10]$; (c) BD~ $[0\bar{1}10]$

Figure 5: (a) SEM image showing as-compressed 4Y-B pillar contains a $(0\bar{1}1\bar{1})$ slip trace; (b) the corresponding TKD result indicates only a small twin exists in the deformed sample.

Figure 6: (a) An overview bright field TEM image showing the primary dislocations lie on the $(0\bar{1}1\bar{1})$ slip plane. (b)-(f) bright field images corresponding to the dashed squared area in (a) under different conditions: (b)(c) BD~ $[11\bar{2}\bar{3}]$; (d)-(f) BD~[0001]

Figure 7: (a) SEM image of the as-compressed pillar 4Y-C showing the (0001) slip trace. (b) TEM bright field image of the as-compressed pillar. (c-d) Bright field images showing basal <a> type dislocations indicated by red arrows. (e-f) Bright field images showing the <c+a> dislocations in contrast in both g vectors of 0002 and $\bar{2}110$.

Figure 8: Dark field image of the <c+a> dislocations in pillar 4Y-C under g=0002 with different tilting angles: (a) 10°; (b) -40°. (c) Schematic drawing showing two Pyra I planes and one Pyra II plane sharing same Burgers vector; (d) Schematic drawing showing

double cross-slip of <c+a> dislocation between Pyra I and Pyra II slip planes resulting zig-zag shape dislocation lines.

Figure 9: Bright field image of <c> component dislocations in the 0.4Y-C compressed pillar with a $(1\bar{2}10)$ section.

Figure 10: Bright field images of <c+a> dislocations in 0.4Y-C pillar with a $(1\bar{2}10)$ section. Different beam conditions are used: (a)(c)(d) BD~$[1\bar{2}10]$; (b), BD~$[0\bar{1}10]$

Figure 11: (a-c) Bright field images of <c+a> dislocations in 0.4Y-C pillar with a (0001) section TEM foil. (a) BD~$[\bar{2}113]$; (b)(c), BD~$[\bar{1}2\bar{1}3]$; (d) Schematic drawing shows a typical <c+a> dislocation loop in Pyra II plane.

Figure 12: The effect of Y content on ratios between CRSS for <c+a> pyramidal slip and CRSS for <a> basal slip in Mg and Mg-Y alloys.

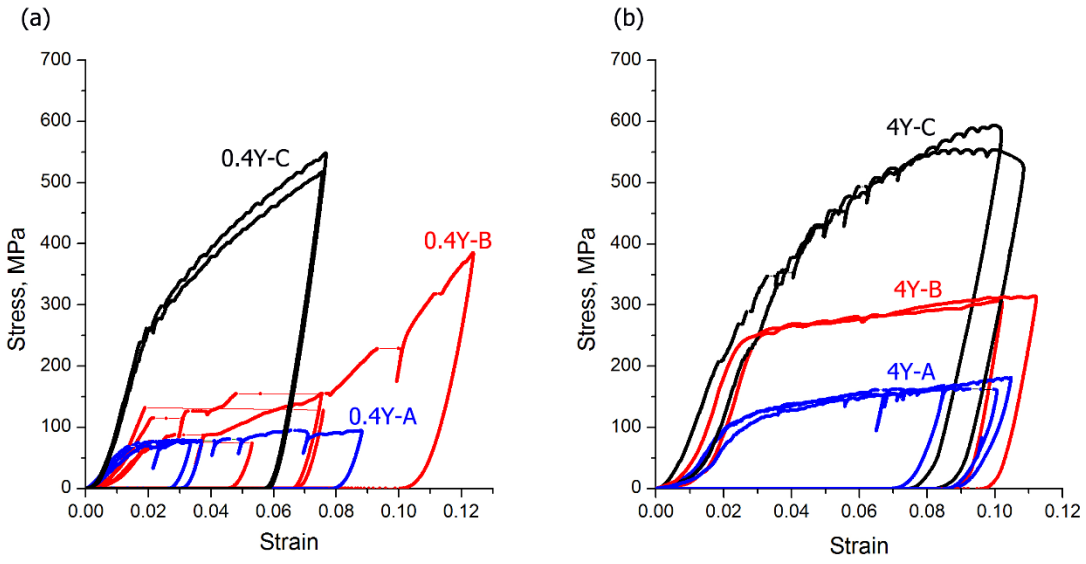

Figure 1

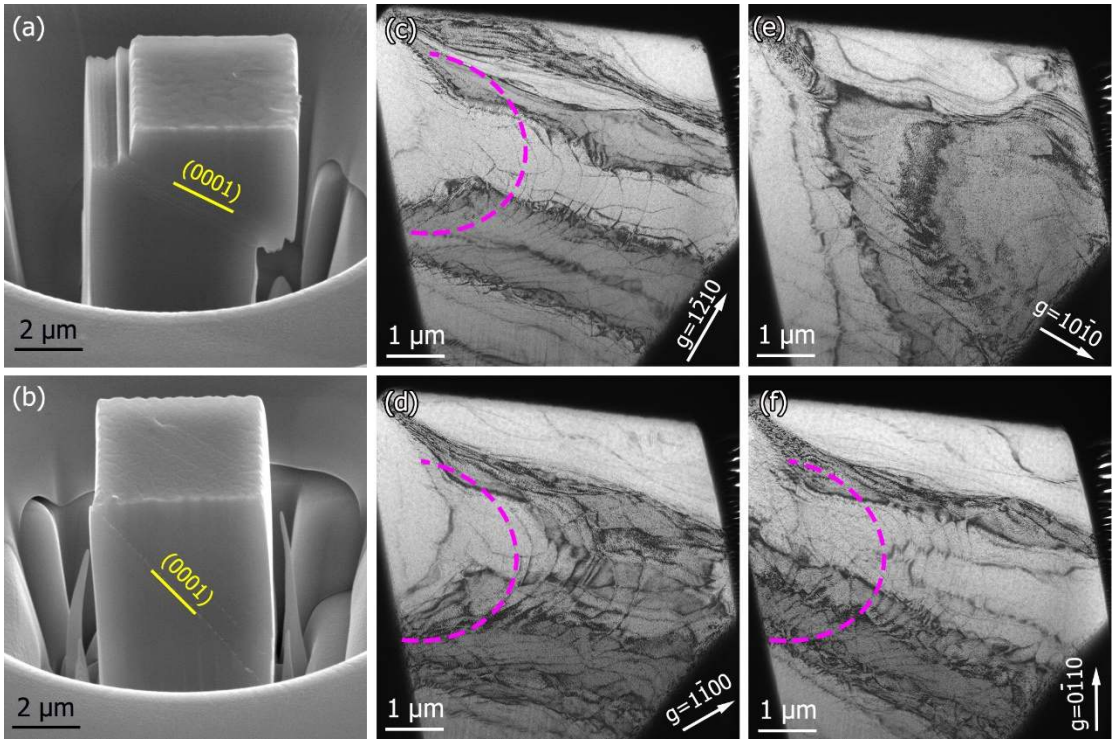

Figure 2

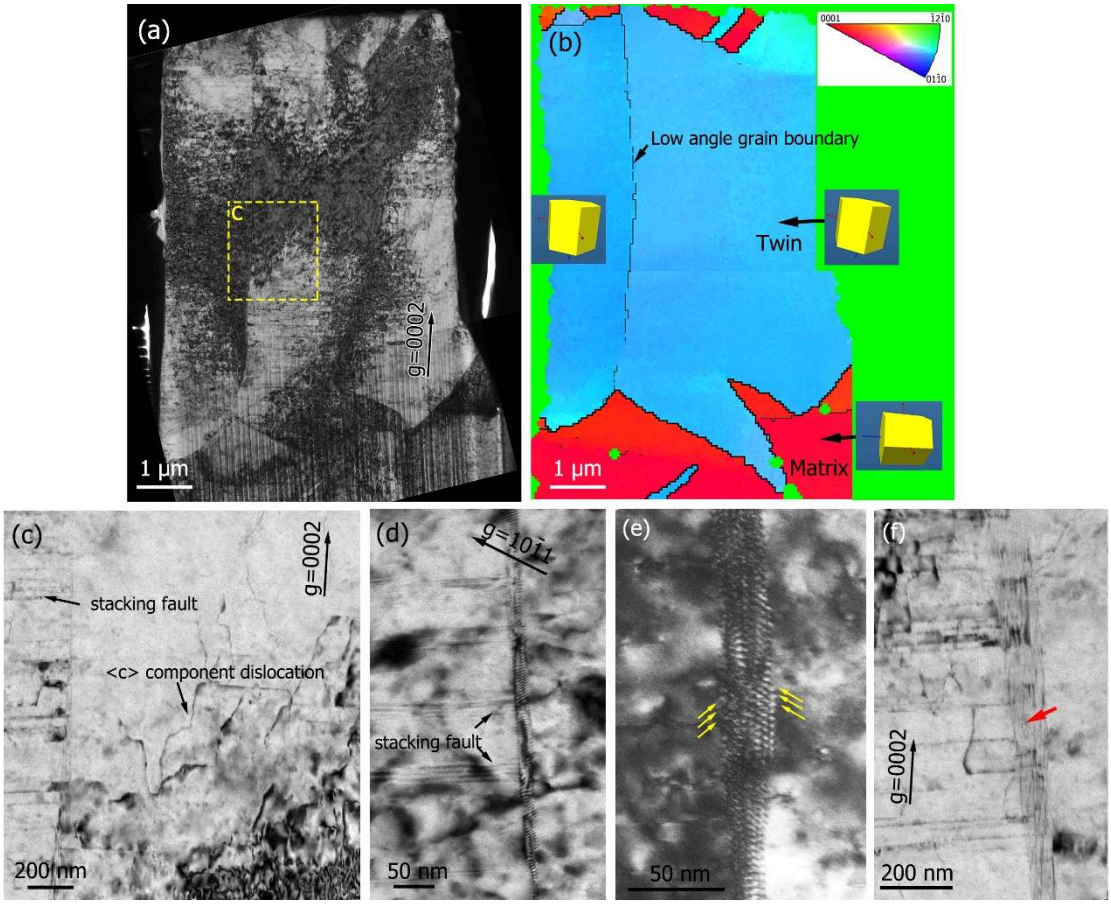
(a)
c
g=0002
1 μm
(b)
0001
$\bar{1}2\bar{1}0$
$01\bar{1}0$
Low angle grain boundary
Twin
Matrix
1 μm
(c)
g=0002
stacking fault
<c> component dislocation
200 nm
(d)
$g=10\bar{1}1$
stacking fault
50 nm
(e)
50 nm
(f)
g=0002
200 nm

Figure 3

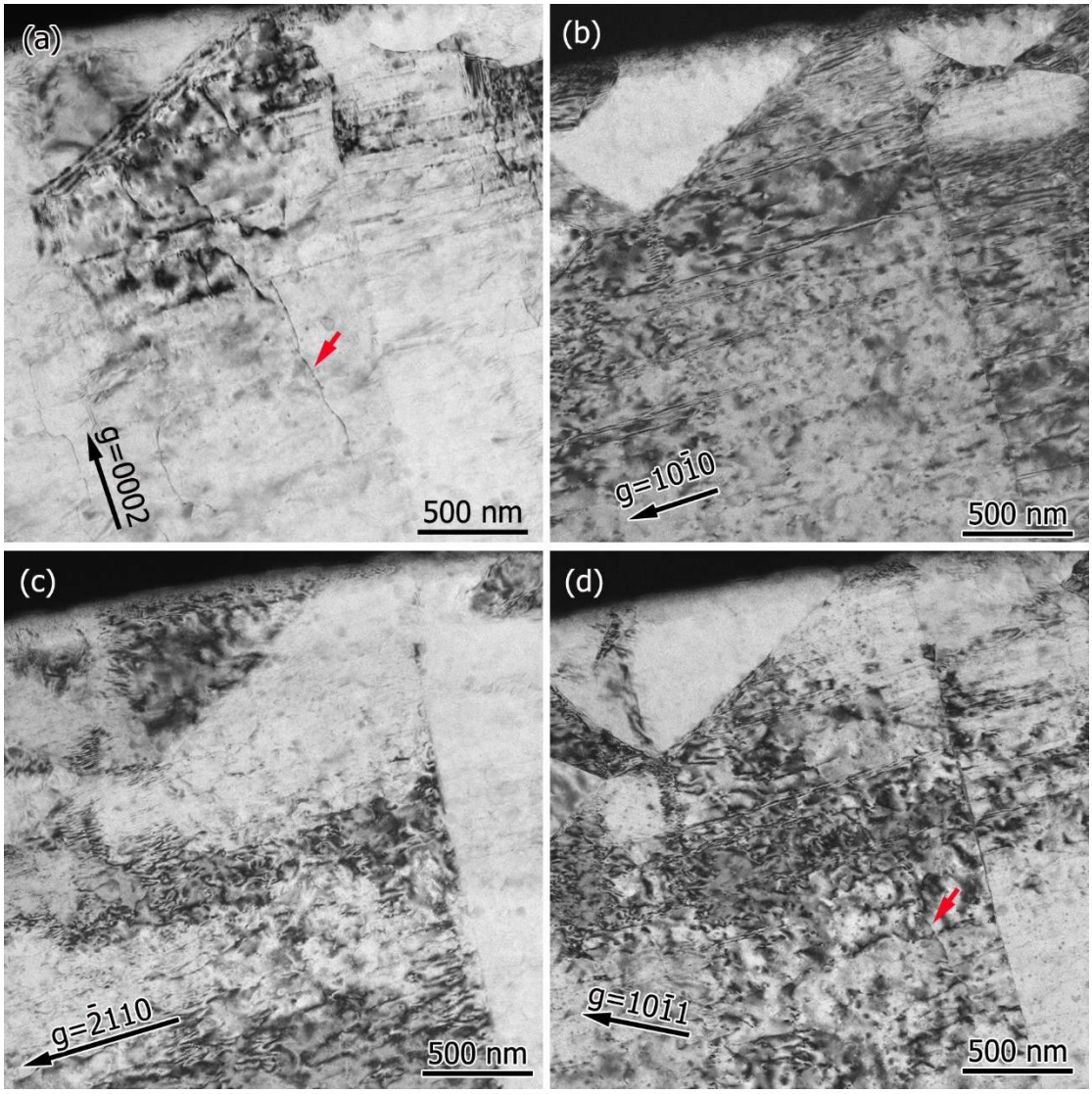

Figure 4

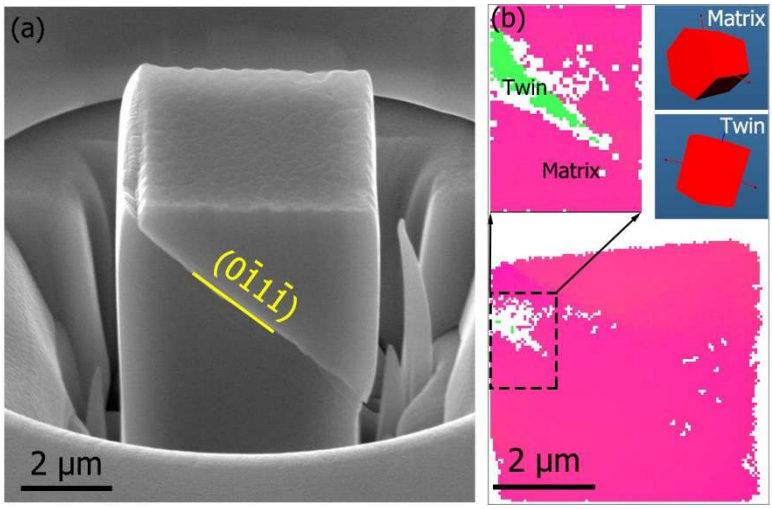

Figure 5

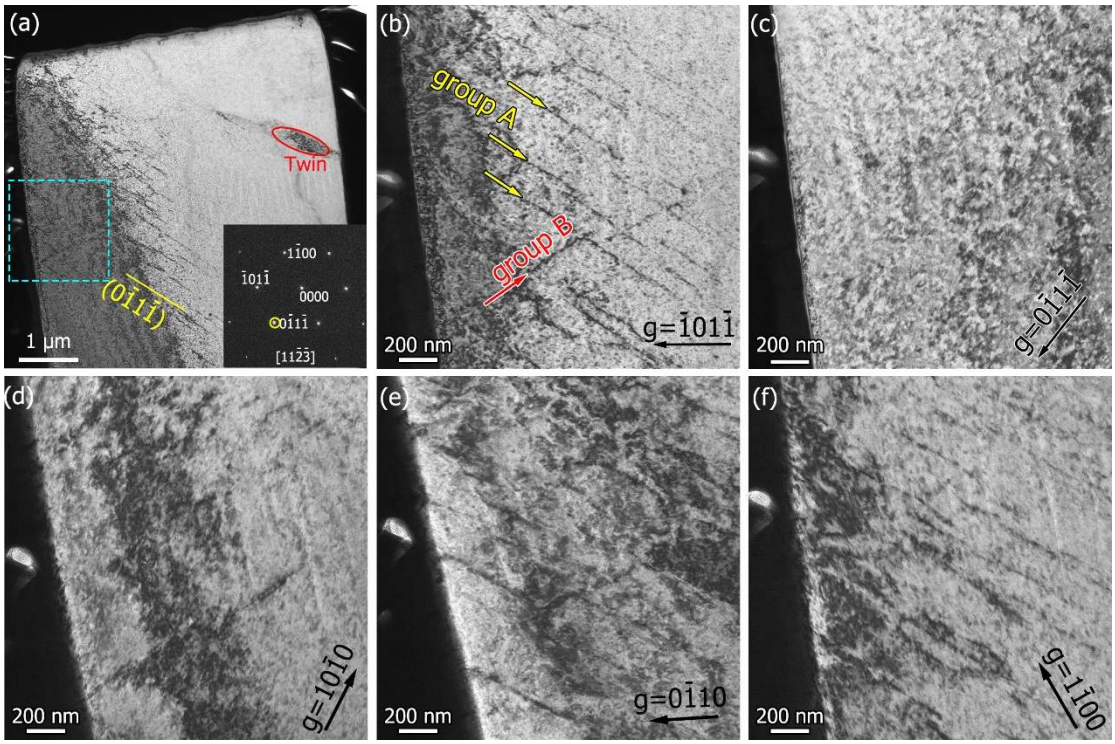
(a)
Twin
(0$\bar{1}1\bar{1}$)
1 μm
$1\bar{1}00$
$\bar{1}01\bar{1}$
0000
0$\bar{1}1\bar{1}$
[11$\bar{2}\bar{3}$]
(b)
group A
group B
200 nm
g=$\bar{1}01\bar{1}$
(c)
200 nm
g=0$\bar{1}1\bar{1}$
(d)
200 nm
g=10$\bar{1}$0
(e)
200 nm
g=0$\bar{1}$10
(f)
200 nm
g=$1\bar{1}$00

Figure 6

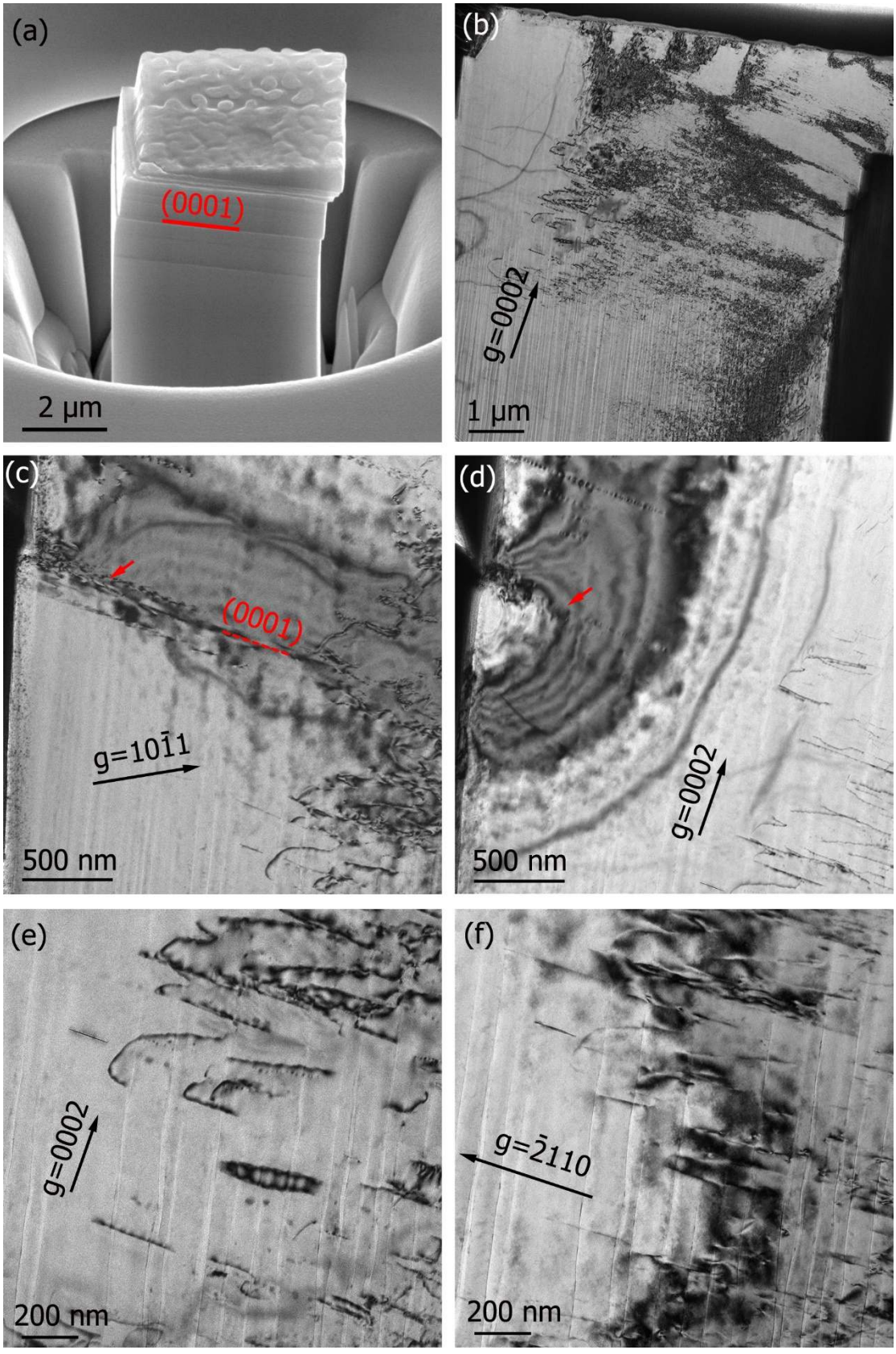
(a)
(0001)
2 μm
(b)
g=0002
1 μm
(c)
(0001)
g=10$\bar{1}$1
500 nm
(d)
g=0002
500 nm
(e)
g=0002
200 nm
(f)
g=$\bar{2}$110
200 nm

Figure 7

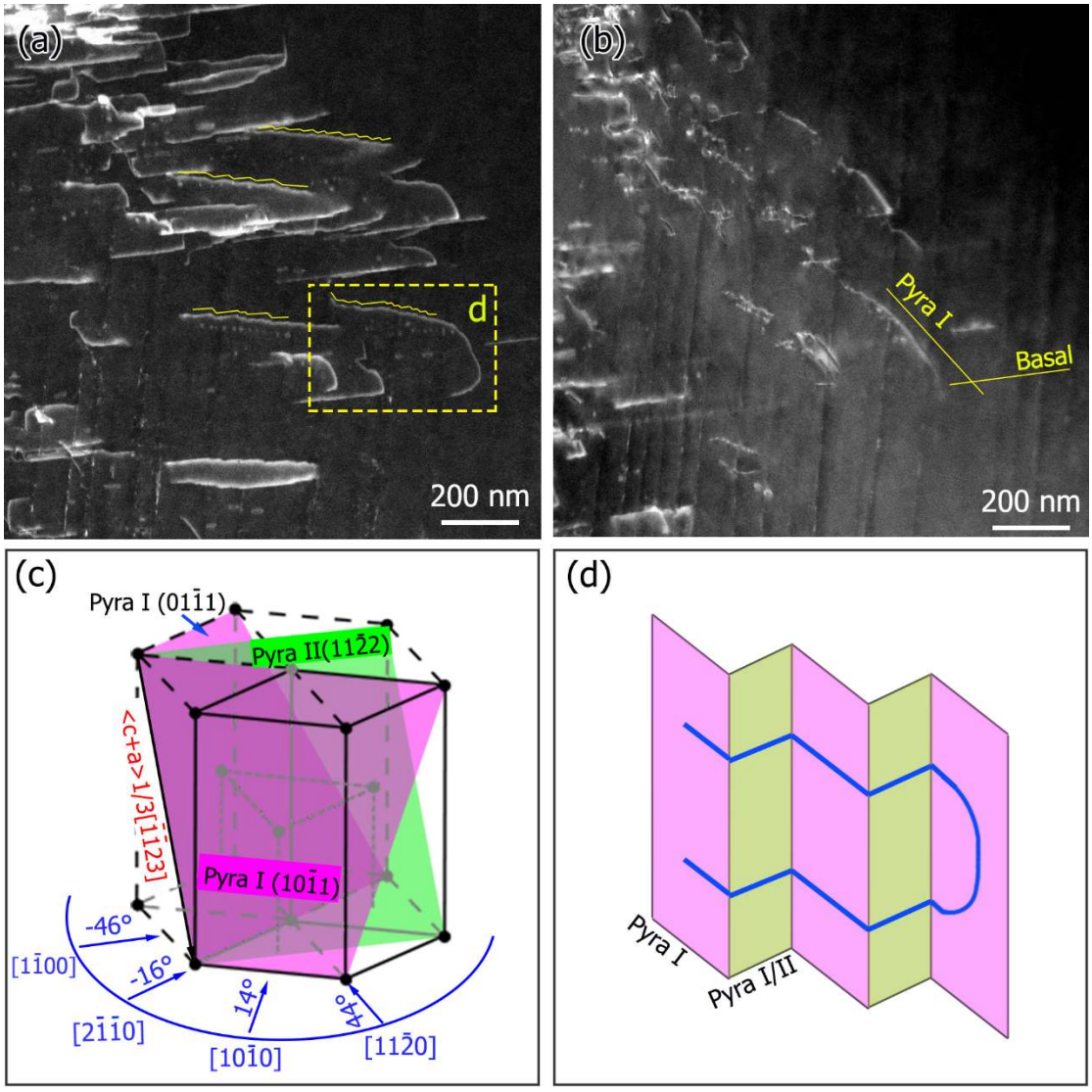
(a)
d
200 nm
(b)
Pyra I
Basal
200 nm
(c)
Pyra I (01$\bar{1}$1)
Pyra II(11$\bar{2}$2)
<c+a>1/3[$\bar{1}\bar{1}$23]
Pyra I (10$\bar{1}$1)
-46°
-16°
14°
44°
[1$\bar{1}$00]
[2$\bar{1}\bar{1}$0]
[10$\bar{1}$0]
[11$\bar{2}$0]
(d)
Pyra I
Pyra I/II

Figure 8

Figure 9

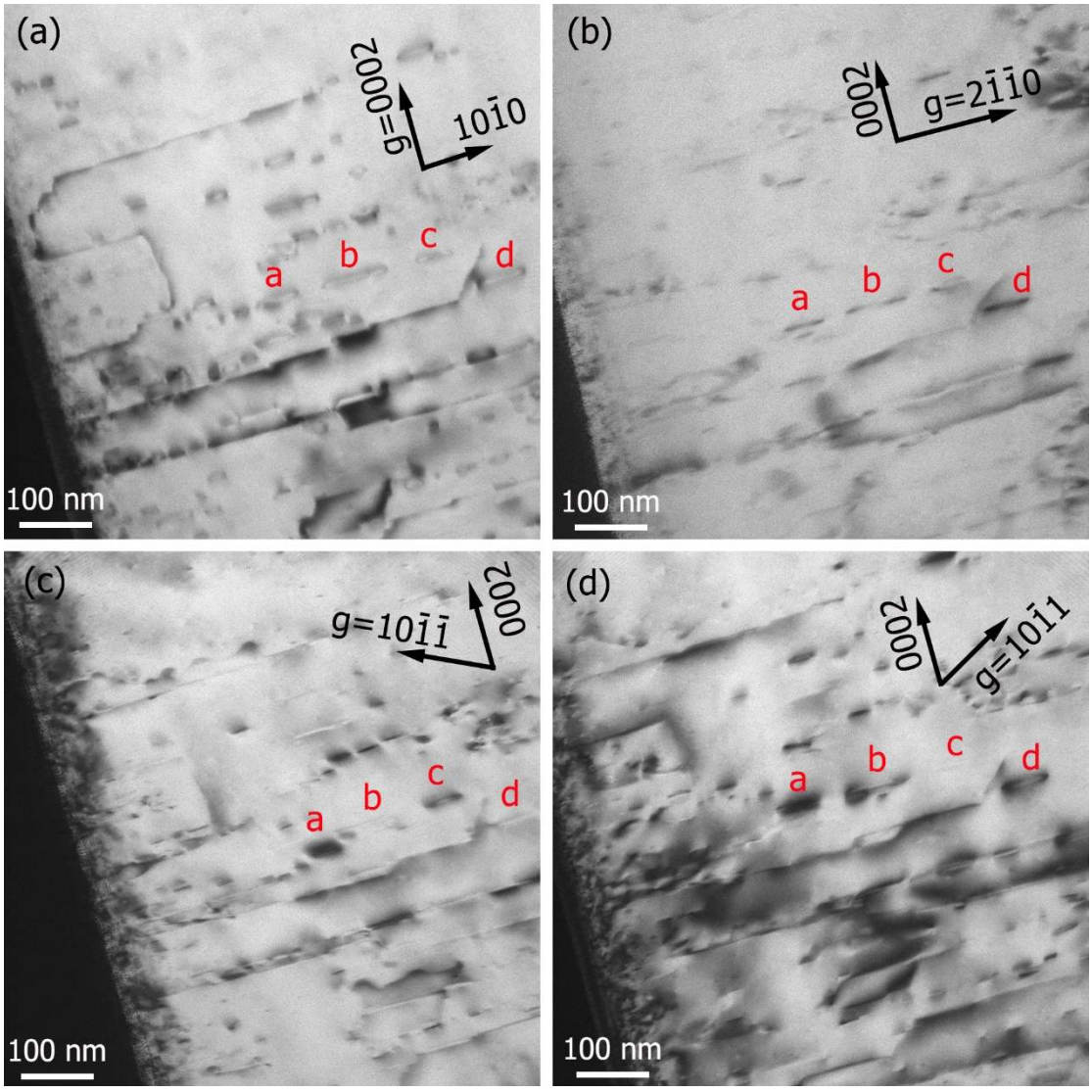
(a)
g=0002
10$\bar{1}$0
a
b
c
d
100 nm
(b)
0002
g=2$\bar{1}\bar{1}$0
a
b
c
d
100 nm
(c)
g=10$\bar{1}\bar{1}$
0002
a
b
c
d
100 nm
(d)
0002
g=10$\bar{1}$1
a
b
c
d
100 nm

Figure 10

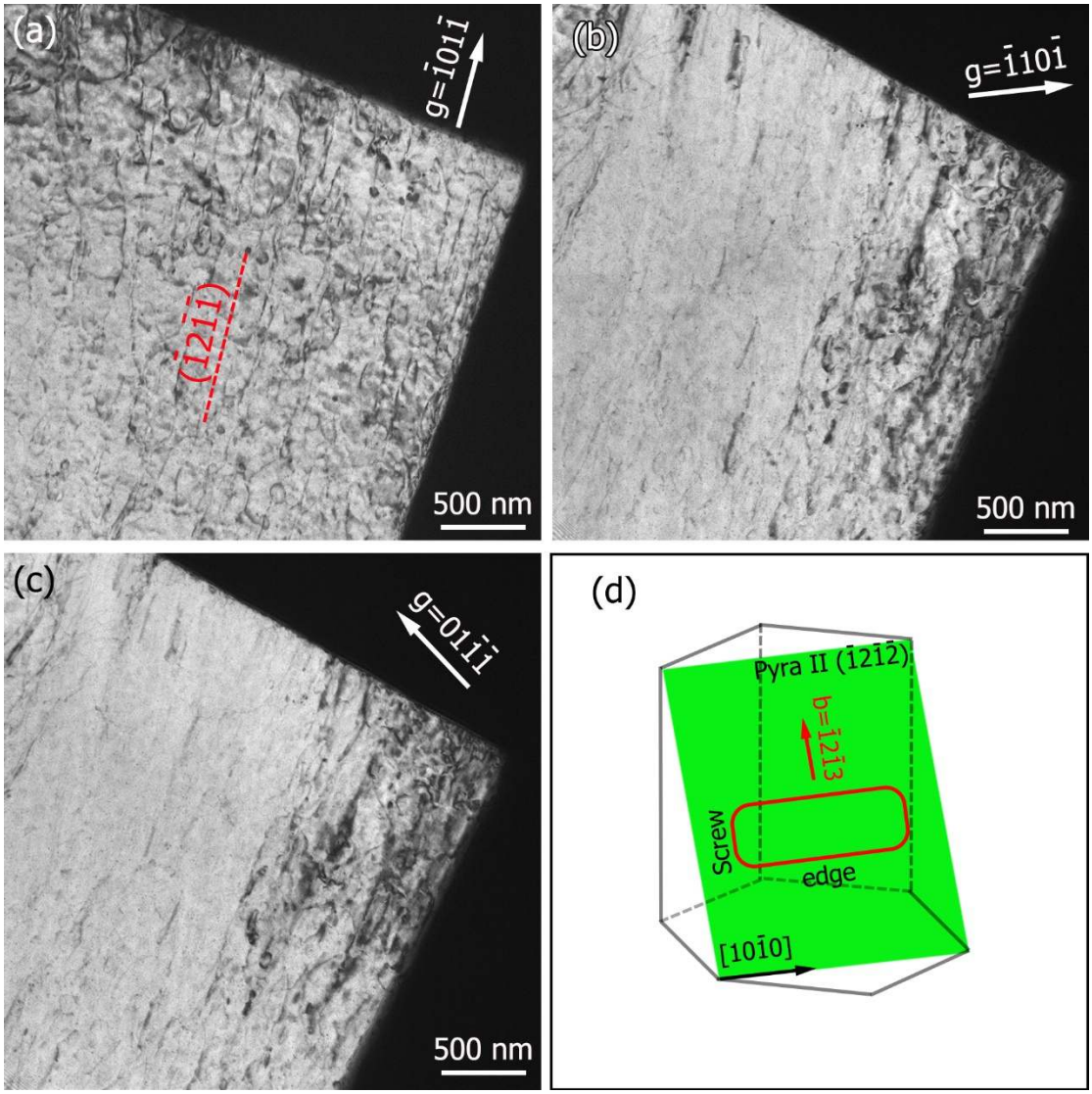

Figure 11

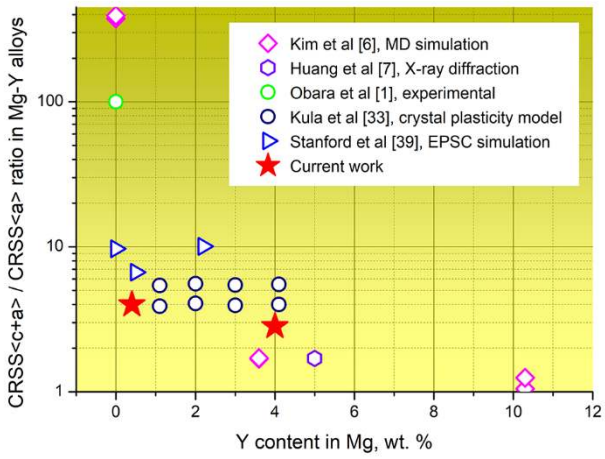

Figure 12